Atypical tuning and amplification mechanisms in gecko auditory hair cells

Maryline Beurg[a], Tony Gamble[b,c,d], Aaron H. Griffing[b], and Robert Fettiplace[a,1]

The auditory papilla of geckos contains two zones of sensory hair cells, one covered by a continuous tectorial membrane affixed to the hair bundles and the other by discrete tectorial sallets each surmounting a transverse row of bundles. Gecko papillae are thought to encode sound frequencies up to 5 kHz, but little is known about the hair cell electrical properties or their role in frequency tuning. We recorded from hair cells in the isolated auditory papilla of the crested gecko, *Correlophus ciliatus*, and found that in both the nonsalletal region and part of the salletal region, the cells displayed electrical tuning organized tonotopically. Along the salletal zone, occupying the apical two-thirds of the papilla, hair bundle length decreased threefold and stereociliary complement increased 1.5-fold. The two morphological variations predict a 13-fold gradient in bundle stiffness, confirmed experimentally, which, when coupled with salletal mass, could provide passive mechanical resonances from 1 to 6 kHz. Sinusoidal electrical currents injected across the papilla evoked hair bundle oscillations at twice the stimulation frequency, consistent with fast electromechanical responses from hair bundles of two opposing orientations across the papilla. Evoked bundle oscillations were diminished by reducing Ca^{2+} influx, but not by blocking the mechanotransduction channels or inhibiting prestin action, thereby distinguishing them from known electromechanical mechanisms in hair cells. We suggest the phenomenon may be a manifestation of an electromechanical amplification that augments the passive mechanical tuning of the sallets over the high-frequency region.

gecko | hair cell | nonmuscle myosin | frequency selectivity | electrical tuning

In all vertebrates, sound stimuli are detected by hair cells in the inner ear, and the frequency constituents of the sound are distributed tonotopically along the auditory papilla to be signaled to the brain by different subsets of auditory nerve fibers. A principal mechanism of frequency analysis in nonmammals is electrical tuning of the hair cell receptor potential based on the activation of large-conductance Ca^{2+} and voltage-dependent K^+ (BK) channels (1–4). However, the upper frequency range of electrical tuning may be limited by K^+ channel kinetics to around 1 kHz (5); consequently, this mechanism is not employed in mammals. Instead, a traveling wave supported by passive mechanical resonances along the basilar membrane is reinforced by amplification via an electromechanical prestin-based motor in the outer hair cells (6); this mechanism encompasses frequencies up to ~100 kHz. Many lizard species have an intermediate frequency range extending to 5 kHz, but the underlying mechanism of frequency selectivity is unclear. Circumstantial arguments have suggested the extended range might be attributable to an active frequency-selective motor in hair bundle transduction (7), as documented in frog saccular hair cells (8, 9). Evidence in support of this mechanism has been the description and modeling of spontaneous otoacoustic emissions (SOAEs), sounds generated by the ear and thought to reflect a hair cell motor. SOAEs are particularly prominent in geckos [the only lizards known to vocalize (10)], where they occur over discrete frequency bands up to 5 kHz (11, 12). Otoacoustic emissions can be produced and manipulated by current injection in the inner ear (7). However, direct evidence for their source has been lacking due to the inability to record from and directly probe the auditory hair cells. Furthermore, there is scant evidence for the contribution of an active hair bundle motor in any other peripheral auditory system (2). One aim of the current work was to investigate possible contributions to frequency analysis of a hair bundle/transduction motor.

Lizard auditory papillae exhibit diverse anatomical arrangements varying in the type of gelatinous structure covering the sensory hair bundles and with the papilla subdivided into multiple zones (13). Like turtles or birds, all lizards possess a region with a continuous tectorial membrane over the hair bundles. Other regions may contain free-standing hair bundles with no tectorial structure, as in the alligator lizard (*Elgaria multicarinata*) (14), or possess "sallets," discrete bands of tectorial material overlying

Author affiliations: [a]Department of Neuroscience, University of Wisconsin Medical School, Madison, WI 53706; [b]Department of Biological Sciences, Marquette University, Milwaukee, WI 53233; [c]Vertebrate Zoology, Milwaukee Public Museum, Milwaukee, WI 53233; and [d]Bell Museum of Natural History, University of Minnesota, Saint Paul, MN 55108

[1]To whom correspondence may be addressed. Email: fettiplace@wisc.edu.

each transverse row of hair cells (Fig. 1 *A* and *B*), as in the Tokay gecko (*Gekko gecko*) (13, 15, 16). The different zones are normally associated with nonoverlapping frequency ranges, the continuous tectorial membrane being confined to frequencies below 1 kHz, where electrical tuning can function, and the variable structures for analyzing frequencies above 1 kHz. Recordings of sound-evoked responses in auditory nerve fibers have indicated a frequency range up to 5 kHz in the Tokay gecko (17, 18). The frequency representation in that gecko has the notable property that the tonotopic map is opposite in polarity to that of other vertebrates: low frequencies are encoded at the base of the papilla closest to the saccule and high frequencies toward the apex (19). The goal of our work was to develop a gecko basilar papilla preparation, optimizing experimental conditions, to facilitate study of the electrical properties and frequency-selective mechanism of the hair cells, including those in the salletal region.

Materials and Methods

Preparation. Recordings were made from hair cells in the isolated basilar papilla of embryonic or recently hatched crested geckos (*Correlophus ciliatus*) that were bred at the Department of Biological Sciences, Marquette University (20). *Correlophus* is a tropical gecko originally dwelling in New Caledonia at temperatures up to 27 °C; the ecology of a similar New Caledonian lizard has been fully described (21). Animals used in this study had a snout-to-tail length of 60 to 90 mm (mean ± SD of 79 ± 9 mm; n = 62) and were between 9 and 13 wk postoviposition. Fertilized eggs (maintained in a Sportsman 1502 incubator; GQF Manufacturing) and recently hatched animals were kept under a 12-h light-dark cycle at 25 to 27 °C. A few mourning geckos, *Lepidodactylus lugubris*, which were smaller than *Correlophus* (mean length, 43 ± 3 mm; n = 5), were also studied. Animals were anesthetized in an induction chamber with isoflurane (22) and killed by decapitation using methods approved by the Institutional Animal Care and Use Committee of the University of Wisconsin-Madison according to current NIH guidelines.
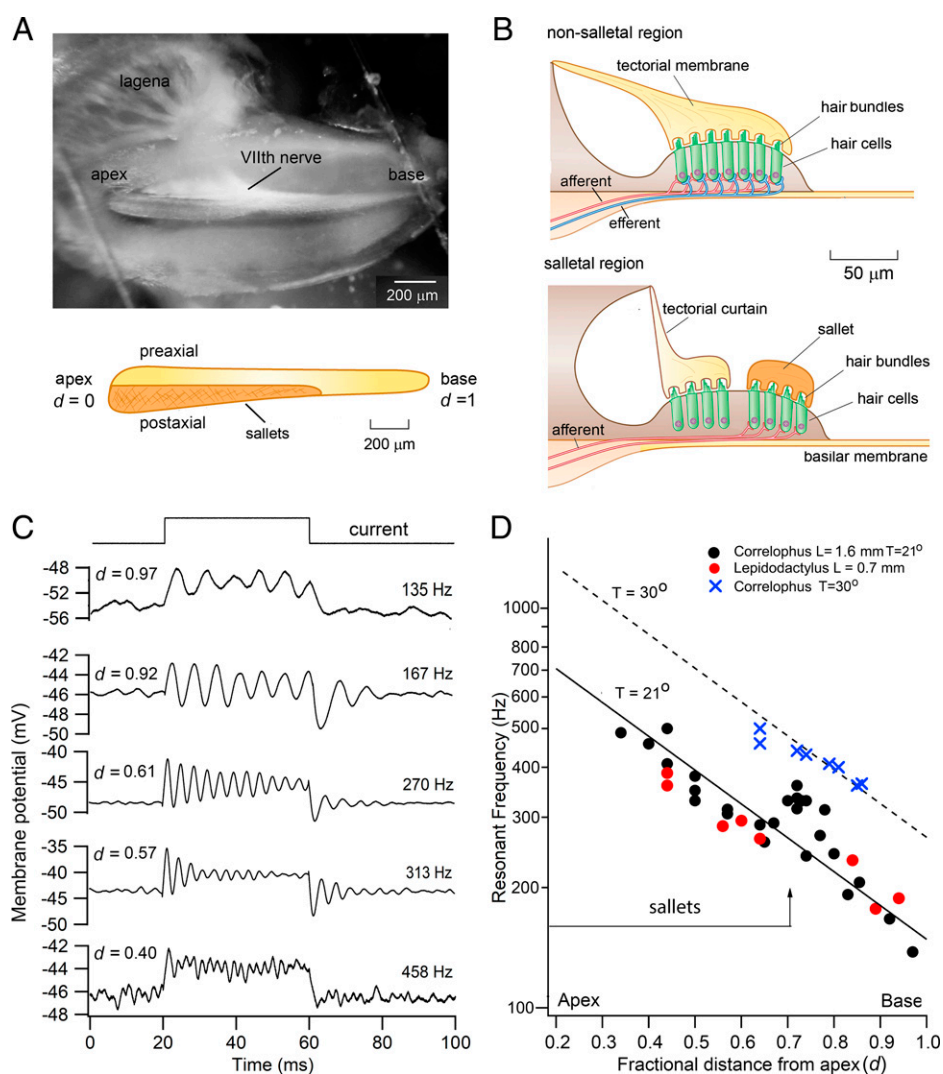

Fig. 1. Electrical resonance in gecko hair cells. (*A*) The gecko auditory organ affixed in the recording chamber with strands of dental floss, seen at the far Left and right of the image, and viewed from the lateral aspect. The hair cell papilla is tapered from apex to base and connects to the auditory branch of the VIIIth nerve; nerve fibers also fan out to the lagena, a vestibular organ. The papilla schematic shown below the image indicates the location of the sallets in the postaxial region. (*B*) Schematics of transverse sections of the papilla at the low-frequency basal nonsalletal region (*Upper*) showing the afferent (red) and efferent (blue) innervation patterns; and near the high-frequency apex (*Lower*), where discrete sallets overlie the abneural hair cells, which have only afferent innervation (16). (*C*) Examples of electrical ringing in hair cells responding to 30- or 60-pA current steps; resonant frequency and cell location are given above each trace. (*D*) Electrical resonant frequency versus hair cell location for *C. ciliatus* (black circles) and *L. lugubris* (red circles) at 21 °C and *Correlophus* (blue crosses) at 30 °C. In this and subsequent figures, cell location is specified by *d*, distance from the apex scaled by total length of papilla (L): mean L = 1.62 mm for *Correlophus* and 0.73 mm for *Lepidodactylus*. Hair cells were recorded after removal of tectorial and salletal membranes. In the salletal region (*d* < 0.7), only postaxial hair cells were sampled, as preaxial cells nearest the neural limb were inaccessible.

The procedure for isolating the basilar papilla was modified from that described for the chicken (23). After removing the jaw, the skull was split along the midline with a razor blade and the otic capsule separated from the skull following section of the VIIIth nerve and severing of the nerve branch to the posterior semicircular canal. The bone over the otic capsule was slowly cracked, the basilar papilla dissected out, and the tegmentum vasculosum removed to expose the intact hair cell epithelium. The initial dissection was performed in HBSS (Hanks' balanced salt solution) supplemented with 10 mM HEPES and 20 mM glucose. In most physiological experiments, the tectorial membrane and tectorial sallets were removed after incubation in HBSS saline containing 50 µg/mL protease type XXIV (Sigma-Aldrich, St. Louis, MO) for 10 min and then terminated by exchange with HBSS saline containing 50 mg/mL bovine serum albumin. The isolated basilar papilla was transferred to the recording chamber and secured, hair bundles uppermost, by two strands of dental floss across the apex and base (Fig. 1A). At the end of each experiment, the distance of the recording site from the apical end of the papilla was measured. This distance was normalized by the total length of the papilla and is expressed as d, the fractional distance from apex.

The experimental chamber holding the preparation was transferred to a Leica DMLFS fixed-stage microscope, where it was viewed through a long working distance ×40 water-immersion objective (numerical aperture, 0.8), a ×2.0 optivar, and a Hamamatsu charge-coupled device (CCD) camera. Videos were obtained from the CCD camera with a frame grabber (The Imaging Source). The chamber was perfused with oxygenized saline composed of 155 mM NaCl, 3 mM KCl, 2.5 mM CaCl$_2$, 10 mM HEPES, 8 mM glucose, and 2 mM Na-pyruvate (pH 7.55, 330 mOsm) at room temperature (21 to 23 °C). Experiments were performed in saline containing 2.5 mM Ca^{2+} instead of the submillimolar Ca^{2+} found in endolymph of other vertebrates, as lizard endolymph may have an unusually high Ca^{2+} (>1 mM) (24). The perfusate in some experiments was heated to 30 °C; the temperature of the bath solution was monitored with a thermocouple (23). Blocking agents (tetraethylammonium chloride [TEA], CoCl$_2$, Na salicylate, dihydrostreptomycin; Sigma-Aldrich) were introduced by addition to the bath after turning off the perfusion system.

Electrical Recordings and Stimulation. Hair cell recordings were made with borosilicate patch electrodes inserted into the abneural edge of the basilar papilla. Patch pipettes were filled with an intracellular solution comprising 137 mM KCl, 0.5 mM BAPTA [(1,2-bis(o-aminophenoxy)ethane-N,N,N′,N′-tetraacetic acid], 3 mM MgATP, 10 mM Tris creatine phosphate, and 10 mM HEPES, pH 7.2, and were connected to an Axopatch 200B amplifier. Series resistance in ruptured patch recordings with up to 70% compensation was 2 to 5 MΩ. Membrane potentials were corrected for current flow across the residual series resistance and for junction potentials (−4 mV for KCl). Hair bundles were mechanically stimulated with a stiff glass probe with a 3-µm tip cemented to a short piezoelectric bimorph (Vernitron, catalog no. PZT-5B). The probe was advanced along the long axis of the papilla and brought up against the abneural edge of the exposed hair bundle to generate transverse bundle displacements. A drawback of the preparation was lack of access to the epithelium from the neural edge of the papilla, due to the tectorial curtain (Fig. 1B), making it impossible to employ a fluid jet stimulator or a local perfusion pipette, as in other hair cell preparations. The bimorph was excited by voltage steps amplified by a high-voltage amplifier and filtered at 1 kHz. In some experiments to determine stiffness, hair bundles were deflected with a flexible glass fiber more compliant than the bundle that was driven by a piezoelectric actuator (16, 25–27). Displacements of the hair bundle or glass probe were calibrated by projecting their image onto a pair of photodiodes (LD 2–5; Centronics) at ×150 total magnification. Freestanding hair bundles were imaged at their tip where they appeared as a bright line (26). The differential photocurrent, which is proportional to the displacement of the object, was calibrated by measuring its amplitude and polarity when displacing the photodiodes a known distance in the image plane, and then using the magnification to determine the equivalent motion in the object plane. In some experiments, hair cells were stimulated en masse by extracellular currents applied using a stimulus isolation unit (A395; World Precision Instruments) connected to two electrodes. One was a 3% agar 3M KCl bridge in contact with a chloridized silver wire placed near the neural side of the papilla; the other was a pipette with a 13-µm-diameter tip filled with extracellular solution and placed ∼100 µm from the abneural edge of the papilla. For assaying hair

bundle motion, responses of single bundles to 100 presentations were averaged at each stimulus level. Movements of the epithelial surface were measured by imaging 2-µm-diameter silica beads (Polyscience) affixed to the epithelium. Results are presented as the mean ± 1 SD and significance assessed by a two-tailed t test.

Immunology. Immunolabeling of cytoskeletal elements was performed in isolated basilar papillae, fixed in 4% paraformaldehyde for 30 min at room temperature, blocked in 10% goat serum for 1 h, and labeled with primary antibodies to α2-spectrin (monoclonal; Thermo Fisher, Waltham, MA), β2-spectrin (monoclonal; Sigma-Aldrich), and the nonmuscle myosin NMIIB (MYH10 gene, polyclonal; Biolegend) all at 1:100 dilution for 2 h at room temperature. Preparations were then labeled with secondary antibodies (rabbit or mouse conjugated with Alexa-488 or Alexa-568, 1:300, 1.5 h) and with Alexa-647 phalloidin, mounted using Fluoromount G and viewed on a Nikon A1 confocal microscope with ×100, 1.4 numerical aperture objective.

Results

Electrical Tuning in Gecko Hair Cells. Damped oscillations in membrane potential indicative of electrical tuning (2) could be evoked by depolarizing current steps in most hair cells (Fig. 1C). Sharp tuning occurred in a membrane potential window between −50 and −40 mV and, in the best recordings, sharply tuned responses were observed at the onset and termination of the current, and spontaneous oscillations were observed in the absence of stimulation. The electrical tuning resembled that seen in turtle, frog, and chicken auditory hair cells (1, 3, 23, 28). The electrical resonant frequency is defined as the frequency at which the tuning is sharpest, corresponding to the largest number of oscillations. Measured frequency values ranged from 135 to 500 Hz at 21 °C and increased exponentially along the papilla from the base (Fig. 1D). A few recordings were made at 30 °C (Fig. 1D), and these signified strong temperature sensitivity with a temperature coefficient (Q$_{10}$) of 2.0, the same as in turtle and chicken (2). Most hair cell recordings were obtained from the crested gecko, *C. ciliatus*, which has an auditory papilla 1.62 ± 0.08 mm (n = 41) in length, but a few recordings were also made in the mourning gecko, *L. lugubris*, with a papillar length of 0.73 ± 0.03 mm (n = 7). Despite the twofold difference in papilla length, the tonotopic maps from the two animals overlaid when expressed as a fractional distance along the organ (Fig. 1D). Two features of the tonotopic map are notable. First, the frequency increased from base to apex, the orientation of the map, therefore, being opposite to that of other vertebrates, for which the highest frequency is at the base. Second, electrical tuning was present in hair cells underlying the sallets as well as those under the tectorial membrane. The salletal region in *Correlophus* extends from the apical tip to 70% of the length to the base (ending at d = 0.72 ± 0.04), but electrical tuning was still evident at d = 0.4. Owing to difficulties with access imposed by the tectorial curtain, it was not possible to characterize hair cells on the neural side of the sallets, sometimes referred to as the preaxial region, to distinguish from the postaxial region containing the sallets (15). Hair cells in the postaxial region are the ones thought to be connected to the afferent terminals (16, 18).

Electrical tuning is subject to the metabolic state of the hair cell and deteriorates with Ca^{2+} loading. The electrical resonance is associated with an oscillation in the intracellular Ca^{2+} (4, 29), and at higher frequencies this requires increased energy consumption. Owing to the greater vulnerability of the high-frequency hair cells, it was not possible to assay systematically their properties or frequency tuning. We were able to characterize electrical tuning for about two-thirds of the papilla but were

not able to make acceptable patch-clamp recordings from the apical third and cannot, therefore, conclude that electrical tuning was absent in the apex. We recorded at a temperature of 21 °C, partially to reduce metabolic stress, but the electrical resonant frequency is temperature dependent (30) (Fig. 1D) and doubles for a 10 °C increase (2). This temperature dependence arises from thermal effects on the gating kinetics of the Ca^{2+}-activated K^+ channel and was previously reported for electrical tuning in both chicken and turtle hair cells (5, 31).

Ionic Currents in Gecko Hair Cells. Depolarizing voltage steps evoked large, voltage-dependent, outward K^+ currents (Fig. 2 A and B) that, for the highest-frequency hair cells recorded, could reach 20 nA (at 0 mV). The outward current was rapidly activating, and its amplitude increased with hair cell resonant frequency (Fig. 2C): the current amplitude at 0 mV, scaled to the membrane capacitance, was directly proportional to resonant frequency (Fig. 2D). This accords with previous observations
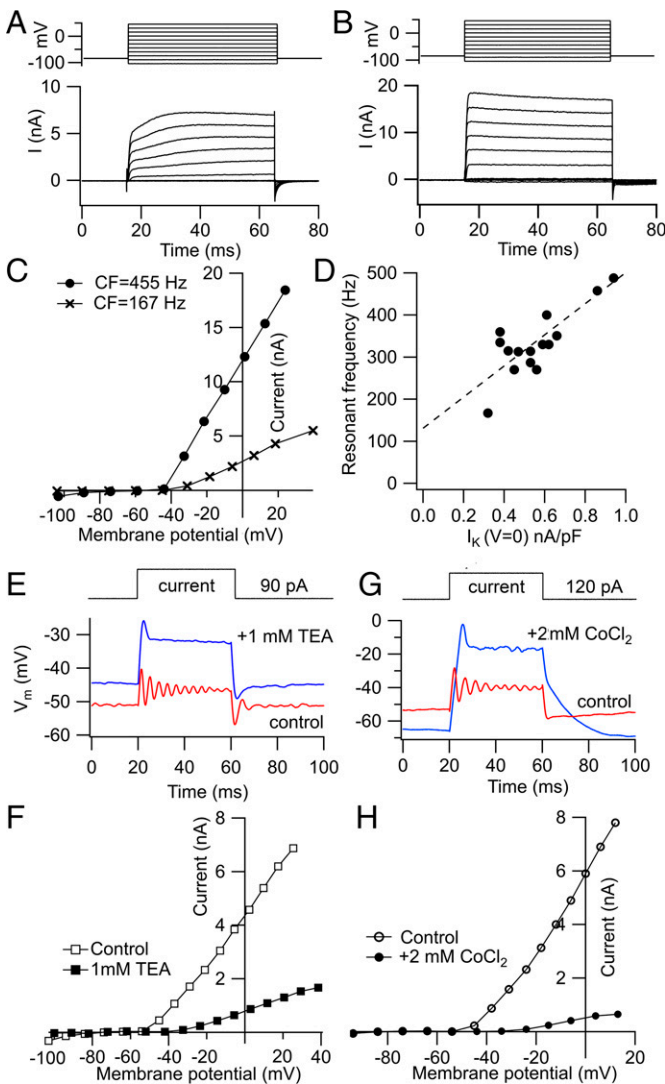

Fig. 2. Membrane currents associated with electrical resonance. (A) Outward currents in a lower-frequency hair cell. (B) Larger and faster outward currents in a higher-frequency hair cell. (C) Current-voltage plots for hair cells in A and B, holding potential −84 mV. CF is the characteristic or resonant frequency of the hair cell. (D) Resonant frequency increases with amplitude of outward K^+ current, measured at 0 mV membrane potential and scaled to cell capacitance. (E and F) Electrical resonance and K^+ current blocked by 1 mM TEA. (G and H) Electrical resonance and K^+ current abolished by 2 mM $CoCl_2$ to block voltage-dependent Ca^{2+} currents.

that the resonant frequency is correlated with the K^+ channel density (29). Addition of 1 mM TEA in three hair cells blocked the voltage ringing (Fig. 2E) and diminished the outward current by $82 \pm 0.01\%$ at 0 mV (Fig. 2F). TEA is known to block BK Ca^{2+}-activated K^+ channels with a K_I of 0.2 mM (32). The membrane resonance in other hair cell systems relies on Ca^{2+} influx through voltage-sensitive L-type Ca^{2+} channels to turn on a BK Ca^{2+}-activated K^+ current (4, 29). L-type (subtype Cav1.3) Ca^{2+} channels are present in salletal hair cells (16) and are blocked by submillimolar concentrations of $CoCl_2$ [$K_I = 0.07$ mM (33)]; at 2 mM, $CoCl_2$ substantially reduced the outward K^+ current and abolished membrane resonance (Fig. 2 G and H). The reduction in the outward current in 2 mM $CoCl_2$ was $77 \pm 15\%$ ($n = 3$) at 0 mV. These features, blocked by low concentrations of TEA and by $CoCl_2$, are consistent with the outward current flowing through Ca^{2+}-activated K^+ channels and with these being the ion channels that underlie electrical tuning in hair cells of the gecko, as in other animals. There is no evidence that either pharmacological agent at these concentrations affects mechanoelectrical transducer (MET) channels (34).

MET Currents in Salletal Hair Cells. MET currents were recorded from gecko hair cells in the salletal region of the papilla and were characterized by step deflections of the bundle imposed with a glass probe driven by a piezoelectric bimorph (*Methods*). We recorded from the two or three most abneural hair cells, because their hair bundles were oriented away from the outer edge of the papilla and so could be excited by displacements toward the neural limb. Evoked MET currents displayed properties like those in other species [turtle (35); rat (36); chicken (23)], including fast adaptation and saturation for displacements exceeding a few tenths of a micrometer (Fig. 3A). For seven salletal hair cells ($d = 0.16$ to 0.58), the peak transducer current in saline with 2.5 mM Ca^{2+} ranged from 0.28 to 0.5 nA (mean = 0.40 ± 0.08 nA), and the mean resting open probability was 0.10 ± 0.04 ($n = 7$). Like other auditory papillae, the MET current size was graded tonotopically (Fig. 3B) (23, 37) and increased in high-frequency cells. The range of MET current amplitudes may stem from a gradient in the number of stereocilia per bundle, as in other vertebrates. Assuming a single-channel current of 6 pA (38) and two channels per stereocilium, a base-apex gradient in the number of tip links per bundle from 24 to 42 was deduced (Fig. 3B).

A gradient in stereociliary number was confirmed by measurements in isolated (unfixed) basilar papillae where, by focusing on the base of the bundles (Fig. 3C), it was possible to determine the stereociliary number by counting the rootlets, demonstrating a range of 30 to 48 from base to apex (Fig. 3F). At the focal plane of the kinocilium, opposite orientations of the bundles were evident across the papilla, as inferred by the kinociliary location on the bundle: the two or three most abneural bundles point inward and the neural bundles point outward (Fig. 3D). The tips of the bundles were inserted into sallets (Fig. 3E), and it should be noted that each sallet connects to oppositely oriented bundles (Fig. 3D). Bundle heights were estimated from the maximum stereociliary lengths when the cells were tilted and viewed on their side, giving bundle heights from 6 to 16 μm, apex to base (Fig. 3F).

Mechanical Resonance. From the number of stereocilia per bundle (N_{SC}) and height (H), it was possible to calculate the overall bundle stiffness, K_{HB}, which equals $(K_R \cdot N_{SC})/H^2$, where K_R is the rotational stiffness of each stereocilium (25)
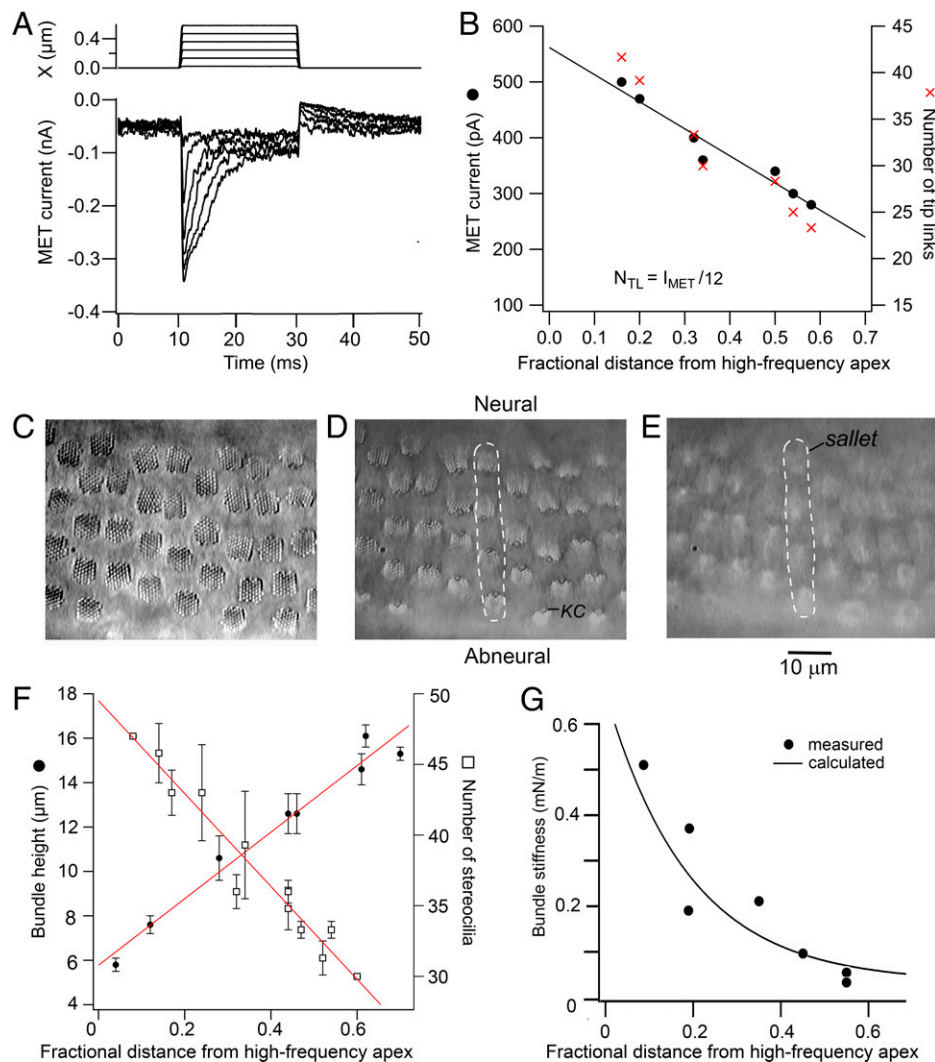
Fig. 3. MET in salletal hair cells. (*A*) MET currents in response to step deflections of the hair bundle (*Upper*) at −84 mV holding potential. (*B*) Tonotopic variation in peak MET current amplitude (black circles) for seven hair cells, and number of tip links (red crosses) derived by assuming each tip link is connected to two 6-pA MET channels. (*C*–*E*) Endolymphatic surface of the abneural aspect of the papilla in the salletal region (*d* = 0.5) focused at three different heights: (*C*) base of bundles, used to count the number of stereocilia; (*D*) top of the bundles, showing the kinocilium (KC), used to determine bundle polarity. Note that in each row of bundles under a given sallet, there is a reversal in bundle polarity about halfway across the papilla. (*E*) The sallets, used to determine the number of hair bundles per sallet; dotted white line emphasizes sallet location. (*F*) Plots of stereociliary number determined from live sections as in *C* and bundle height determined from tallest stereocilia when the cell was pushed on its side. Each measurement, ±SD, was made on four hair bundles, including oppositely oriented polarities, at each location in two preparations. (*G*) Tonotopic variation in hair bundle stiffness versus cell location. Smooth curve was calculated (*Results*) from bundle height and number of stereocilia assuming the rotational stiffness of a stereocilium as 4.6 × 10⁻¹⁶ N.m/rad. Filled circles are discrete measurements on single hair bundles, as described in *Methods* (25).

and is 4.6×10^{-16} N.m/rad. From tonotopic variations in bundle height and stereociliary number (Fig. 3*F*), the gradient in bundle stiffness along the papilla was calculated and was verified by direct measurements on individual bundles (Fig. 3*G*, smooth curve and filled symbols), confirming an ∼12.5-fold change in bundle stiffness. The stiffness for radial motion of each sallet when attached to the row of hair bundles is determined by the stiffness of the attached bundles and the number of hair bundles affixed to each sallet. This number ranged from 2.1 ± 0.8 at the base ($d = 0.7$) to 5.0 ± 1.0 at the apex (extrapolated to $d = 0$). Therefore, the stiffness of each sallet attached to the row of hair bundles increases ∼30-fold from base to apex, i.e., from lower to higher frequencies.

The stiffness of the bundle/sallet combination can, in theory (39), generate a mechanical resonance of frequency (F_M) given by $F_M = (K_i/M)^{0.5}/2\pi$, where M is the mass of the sallet and K_i its stiffness when attached to multiple hair bundles (Fig. 4*A*). With constant salletal mass, the stiffness variation generates a

5.7-fold change in mechanical resonance. Based on a hemispherical sallet of volume 1,600 μm³ and tectorial density of 1.27 g/mL (40), a salletal mass $M = 1.9 \times 10^{-12}$ kg (2) can be derived, and the inferred frequency range is 1.1 to 6.2 kHz. Fig. 4*B* shows the tonotopic gradient in the mechanical resonant frequency and the electrical resonant frequency, the latter having been corrected to 27 °C based on a Q_{10} of 2.0 (Fig. 1*D*). These are superimposed on the tonotopic organization deduced from auditory nerve recordings in Tokay geckos (19). In a first analysis, it was assumed that each sallet oscillates independently, though this may not be the case (12).

Electromechanical Responses of Salletal Hair Cells. The combination of salletal stiffness and mass may confer a passive mechanical resonance on the hair cell input (39), but this is likely to be heavily damped by viscous drag in the absence of local amplification. We investigated possible amplification mechanisms by measuring the motion of individual hair
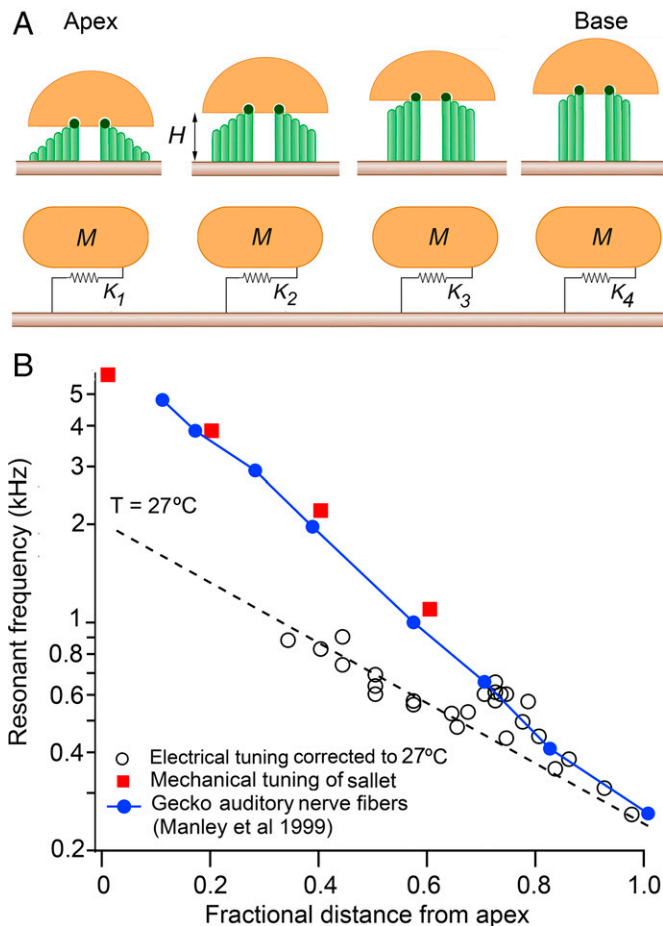
Fig. 4. Tonotopic arrangement of electrical and mechanical tuning in the gecko papilla. (*A*) Mechanical resonance of sallets calculated from mass of sallet (M) and stiffness of attached hair bundles (K_i) for four locations: $d = 0$, 0.2, 0.4, and 0.6. (*B*) Comparison of tonotopic variation in electrical resonant frequency, corrected to 27 °C (open circles), and mechanical resonance (red squares) with characteristic frequencies of labeled auditory nerve fibers recorded in Tokay gecko at 27 °C (blue circles), taken from ref. 19.

bundles with sallets removed in response to extracellular electrical stimuli applied across the hair cell epithelium (25, 27, 41). We focused on the apical half of the papilla containing cells tuned to higher frequencies. Sinusoidal transepithelial currents at frequencies of 50 to 800 Hz evoked hair bundle motion often at twice the stimulation frequency (Fig. 5*A*). The amplitude of bundle displacements saturated with increasing current amplitude and declined with frequency to half the maximum amplitude at ~500 Hz (Fig. 5*B*), which corresponds to a time constant of 0.32 ms. Maximum bundle excursions in response to transepithelial currents ranged from 10 nm to greater than 100 nm ($n = 48$). The voltage-evoked movements were reversibly diminished by reducing the Ca^{2+} influx (Fig. 5 *C* and *D*) by two different methods, and the results were specified by R_T, the ratio of the test displacement relative to the controls before and after. Block of Ca^{2+} influx by adding 2 mM $CoCl_2$ to extracellular saline gave $R_T = 0.29 \pm 0.09$ ($n = 5$; paired *t* test, $P = 0.05$); altering the divalent content of the external saline to 0.2 mM Ca^{2+} + 2 mM Mg^{2+} gave $R_T = 0.31 \pm 0.05$ ($n = 6$; paired *t* test, $P = 0.02$). The bundle oscillations for transepithelial currents are unlikely to stem from effects on the MET channels (Fig. 5*E*) since evoked motion was insensitive to 0.2 mM of the MET channel blocker dihydrostreptomycin (42, 43) ($R_T = 1.01 \pm 0.06$; $n = 5$; paired *t* test, $P = 0.39$).

Imaging of the papilla revealed that transepithelial currents caused each hair bundle to tilt along the neural–abneural axis

(*SI Appendix* and Movie S1); cells with different bundle polarities across a row generated motion in opposite directions. Two properties testify to the biological origin of the evoked movements. First, they often ran down with time, more quickly with larger applied current stimuli. Second, in each field, movements were evident in some bundles but not in others, indicating cellular variation. To examine further the different polarities of motion, we combined administration of transepithelial electrical currents with fluid jet simulation of the hair bundle (Fig. 5 *F* and *G*). The fluid jet was introduced from the abneural surface of the papilla, and the initial phase of bundle motion was in the direction of the neural limb, toward the kinocilium for cells on the papilla's outer edge (Fig. 5*F*) and away from the kinocilium for cells on the inner edge of the papilla (Fig. 5*G*). This allowed us to define the polarity of the photodiode signal. The initial phase of bundle motion with transepithelial electrical currents was in the opposite direction for the two bundle orientations. Thus, for both bundle orientations, negative currents caused motion toward the kinocilium, which is normally associated with MET channel opening. This observation sets limits on the type of underlying mechanism, requiring it to be associated with a cellular asymmetry. It cannot, for example, be caused by the outer hair cell motor prestin, which, if uniformly distributed, would elicit the same direction of feedback in both cell orientations (7). In accord with this conclusion, voltage-evoked displacements were not significantly affected by a prestin inhibitor, 20 mM Na salicylate (44) ($R_T = 0.90 \pm 0.02$; $n = 5$; paired *t* test, $P = 0.11$).

If all hair cells across a row are depolarized equally by the transepithelial current, the differing electrical responses according to bundle orientation can account for the second harmonic response. Hair bundles oriented in one direction contribute one phase of the response, while those oriented in the opposite direction respond with the opposite phase. This would be possible if the evoked bundle response is mediated by motion of the epithelial surface of the papilla, mechanically coupling adjacent cells. However, it could, in theory, also arise by fluid coupling between neighboring bundles. The possibility of mechanical coupling was examined by simultaneously observing transverse motion of silica beads affixed to the epithelial surface between adjacent bundles (Fig. 6 *A* and *B*). In four experiments, motion of the beads to transepithelial currents also displayed a second harmonic response of amplitude similar to the tip of the bundle. In Fig. 6*A*, the bead on the reticular lamina was 2 μm in diameter, much smaller than hair bundle heights of 10 μm at this location. Fluid flow from motion of adjacent bundles is likely to be small near the base of the bundle and probably insufficient to move the bead by the same amount as the tip of the bundle.

The polarity and extent of the induced hair cell polarization were established by simultaneous patch-clamp recording from individual hair cells during passage of transepithelial currents. Depolarizing currents injected through the patch electrode evoked hair cell ringing from a resting potential of about −50 mV (Fig. 6*C*). Extracellular currents produced with the abneural electrode positive also depolarized this hair cell and generated voltage oscillations (Fig. 6*D*). The depolarization increased with the extracellular current amplitude (Fig. 6 *D* and *E*), with a proportionality constant of 71.3 ± 1.6 mV/mA ($n = 6$). Comparing amplitude results in Figs. 5*B* and 6*E* indicates that bundle displacements away from the kinocilium are elicited by 30 to 40 mV depolarizations of the hair cell, conferring a negative feedback action on transduction.

Voltage-evoked deflections of hair bundles have been reported in vestibular hair cells (45, 46). One intriguing
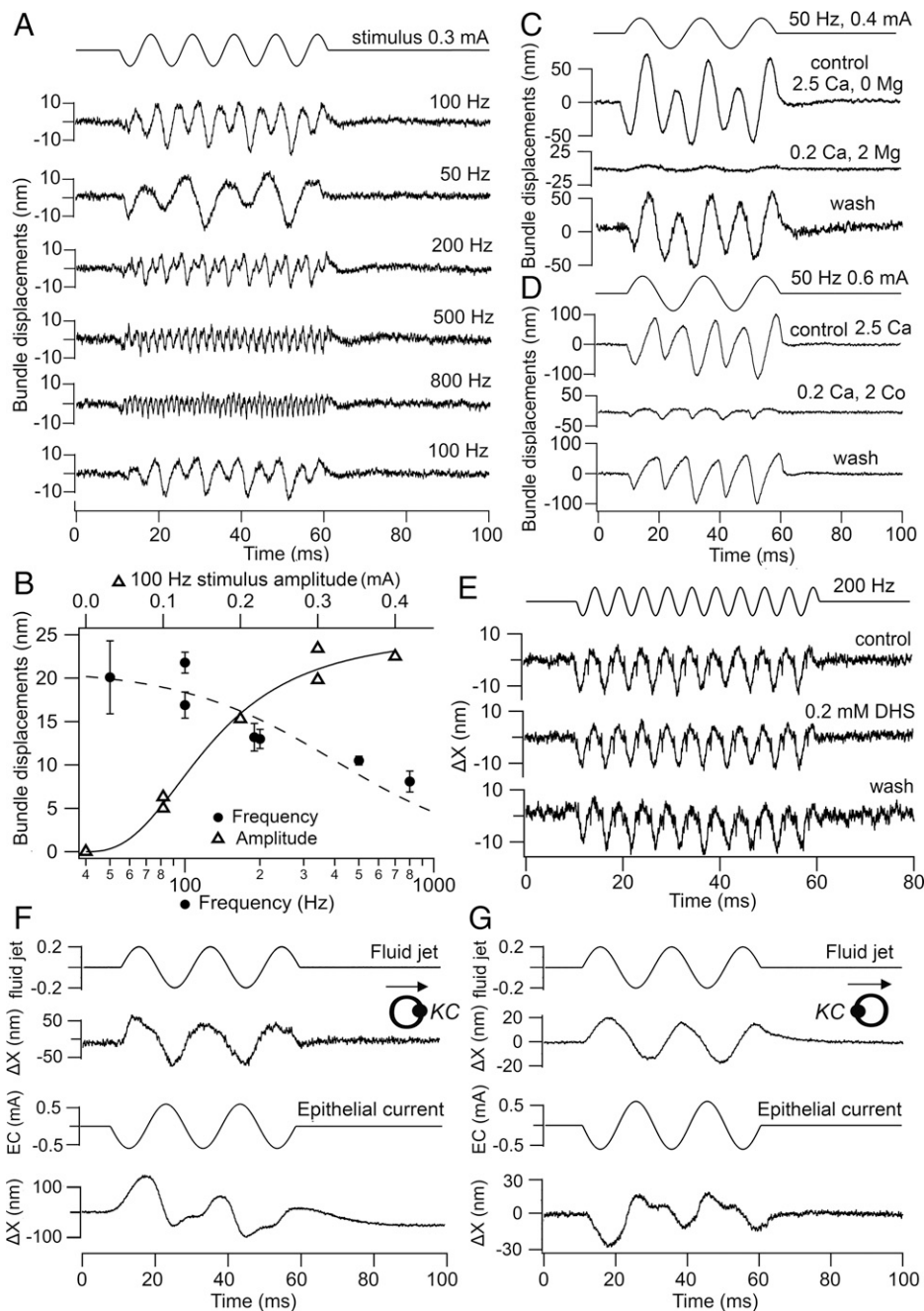
Fig. 5. Electromechanical phenomena in salletal hair cells. (*A*) Hair bundle motion evoked by 0.3-mA sinusoidal extracellular currents passed across the papilla. Current frequency was changed from 50 Hz to 800 Hz bracketed by 100 Hz at the beginning and end of the run. The stimulus monitor (*Top*) is solely for 100 Hz, other frequency stimuli having the same duration. Note the response occurred at twice the stimulus frequency. (*B*) Mean bundle motion (±SD) versus stimulus frequency fit with a Lorentzian of 500 Hz half-power frequency (filled circles); bundle motion increased and then was saturated with increasing size of the command extracellular current (triangles). (*C*) Evoked bundle movements were reversibly blocked by lowering Ca^{2+} influx, reducing extracellular Ca^{2+} from 2.5 to 0.2 mM and adding 2 mM Mg^{2+} (*Top*) or (*D*) 2 mM Co^{2+}. (*E*) Evoked bundle movements were unaffected after 12-min exposure to 0.2 mM MET channel blocker dihydrostreptomycin (DHS). The bottom trace, wash after 10 min, is a noisier single trace than the top two traces, which are averages of two responses. ΔX is hair bundle displacement. (*F*) In an abneural hair cell with the bundle pointing toward the neural edge, bundle motion caused by fluid jet stimulus (*Top Pair*) is compared with motion elicited by extracellular current (*Bottom Pair*). Initial phase of bundle motion to fluid jet stimulus and to current were both toward the kinocilium (KC). (*G*) For another neural hair cell with the bundle pointing toward the abneural edge, the initial phase of the bundle motion to current was opposite to that caused by the fluid jet. For both abneural (*F*) and neural (*G*) hair bundles, negative extracellular current generated bundle motion toward the KC. All measurements were made on exposed hair bundles after removal of sallets. EC, epithelial current.

possibility is that the motor originates with the basal body or the striated organelle harboring the requisite asymmetry, linking the stereociliary rootlets and lateral hair cell membrane (47). We examined the distribution of cytoskeletal elements α2- and β2-spectrin, which are associated with the striated organelle (47) and nonmuscle myosin NMII, suggested to regulate cell tension around the hair cell apical

surface (48). Both α2- and β2-spectrin labeled the luminal hair cell surface (Fig. 7 *A–C*) and depicted well the opposing orientations of the hair bundles. No labeling was observed for NMIIA, but NMIIB (also known as MYH10) exhibited a bead-like appearance on the kinocilium and, in the cell soma, was confined to the region of the basal body on the kinociliary aspect of the hair cell (Fig. 7*D*). Its
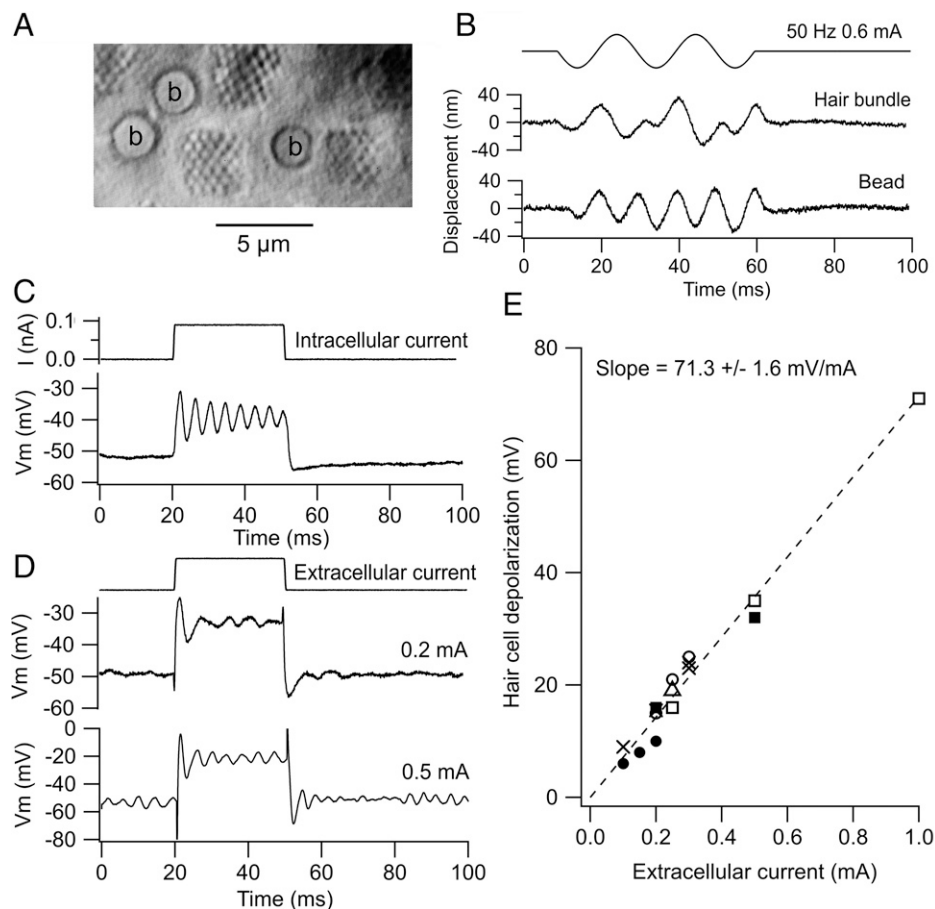
Fig. 6. Motion of epithelial surface and hair cell voltage responses during transepithelial currents. (*A*) Image at the base of the hair bundle, showing placement of 2-μm silica beads (labeled b). (*B*) Transepithelial currents, 50 Hz, 0.4 mA, evoked motion of a hair bundle and adjacent bead, both displaying second harmonic motion. (*C*) Depolarizing current injected through a patch electrode generated an electrical resonant voltage response. (*D*) Positive extracellular current across papilla depolarized the same hair cell as in *C* (*Upper*) and another hair cell (*Lower*) at a similar location, causing oscillatory voltage responses. (*E*) Hair cell depolarization in six cells is proportional to the size of the positive extracellular current. Slope = 71.3 ±1.6 mV/mA. Location, *d* = 0.5. All measurements were made on exposed bundles of salletal hair cells after removal of sallets.

presence was, therefore, polarized, unlike in mammalian hair cells (48).

Discussion

We developed an isolated auditory papilla of the crested gecko lizard, allowing us to record from hair cells in both the lower-frequency tectorial and higher-frequency salletal regions of the epithelium in situ. Geckos are of interest because of the unique arrangement of discrete sallets covering the hair bundles in the high-frequency region of the papilla. Two major findings are the presence of electrical tuning in both tectorial and salletal hair cells and a process of voltage-controlled bundle movements, conceivably underlying amplification, in higher-frequency salletal cells. As with other nonmammalian amniotes, an electrical resonance (1, 2) underlies the tuning of low-frequency hair cells, which, when extrapolated to 27 °C, extends to at least 1 kHz. A limitation of our measurements was an inability to obtain satisfactory recordings from high-frequency hair cells, tuned between 1 kHz and 5 kHz, in the apical third of the papilla. Consequently, we were unable to determine whether electrical tuning still functions in these cells. However, an alternative mechanical resonance may operate in the high-frequency hair cells, conferred by the hair bundle stiffness and the salletal mass (39). The stiffness of the bundle/sallet combination increases about 30-fold from base to apex and,

with constant salletal mass, the inferred frequency range is 1.1 to 6.2 kHz.

A significant observation was that hair bundle oscillations could be evoked by currents passed across the papilla to change the hair cell membrane potential. We suggest this electromechanical phenomenon may underlie amplification of the passive mechanical resonance. The phenomenon is unlikely to be an artifact of gross deformation of the papilla, because imaging showed a variability between adjacent cells, and cells with different hair bundle orientations had opposite polarities of evoked motion. Both arguments suggest that individual hair cells are the site of force generation. Two mechanisms of electromechanical feedback have previously been described in hair cells. One has been largely characterized in bullfrog saccular hair cells and depends on activation and adaptation of the MET channels (8, 9). In the bullfrog saccule, hair bundle oscillations can also be elicited by transepithelial currents, but these oscillations are abolished by the aminoglycoside antibiotic gentamicin, a blocker of the MET channels (41), whereas in the gecko, voltage-evoked bundle movements were insensitive to dihydrostreptomycin, another aminoglycoside antibiotic. A second electromechanical mechanism involves prestin, a membrane motor protein underlying somatic contractions of mammalian outer hair cells (6, 49, 50). Somatic contractions of outer hair cells are abolished with the prestin inhibitor salicylate, which had no effect on voltage-evoked motion of gecko
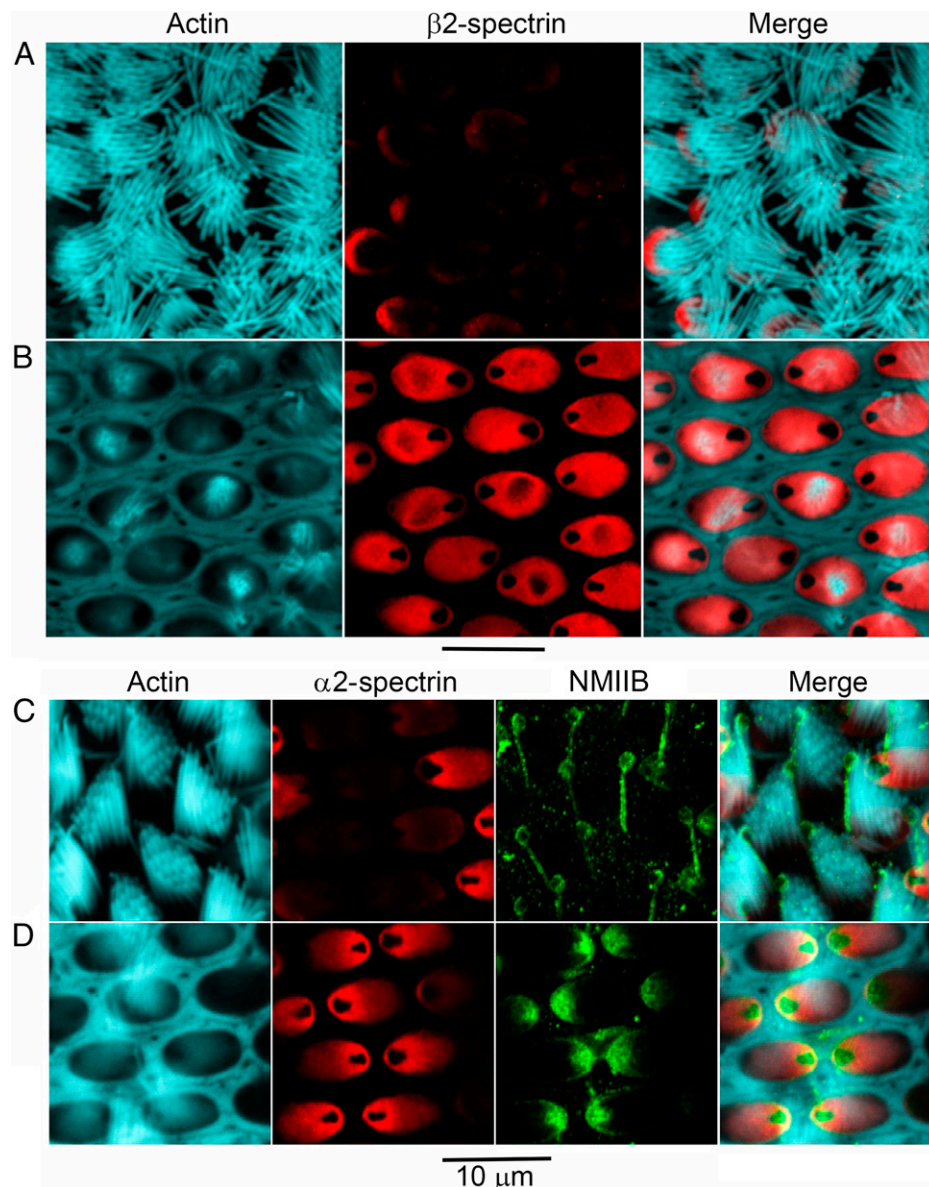
Fig. 7. Immunolabeling for spectrins and nonmuscle myosin IIB (MYH10). (*A*) Labeling of actin and β-spectrin with focal plane at top of bundle. (*B*) Labeling of both at bottom of the bundle, with phalloidin labeling of actin showing the tight ring of supporting cells. (*C*) Labeling of actin, α-spectrin, and NMIIB at top of the bundle. (*D*) Labeling at bottom of the bundle on the hair cell luminal surface, where NMIIB was confined to the kinociliary aspect of the cell. (Scale bars, 10 μm.).

hair bundles. Thus, from a pharmacological standpoint, neither previously reported process can account for the motor in gecko hair cells.

While the precise molecular mechanism is unknown, the process has the advantage of explaining how hair bundles pointing in opposite directions can act synergistically. For a deflection of the sallet toward the abneural edge of the papilla, the neural and abneural bundles will generate depolarizing and hyperpolarizing receptor potentials, respectively, which will drive active motion of the bundles in the same direction. For other mechanisms, the active bundle movements from the neural and abneural cells would work against each other (7). For example, if the electromechanical process involved prestin, neural cells that were depolarized by the sensory stimulus would contract, whereas abneural cells hyperpolarized by the sensory stimulus would elongate. The cooperative action of the oppositely oriented neural and abneural cells may be germane to the operation of hair cells in vestibular maculae with their line of polarity reversal around the striola.

We suggest the atypical process we have described depends on membrane potential, with a voltage range from a resting potential of approximately −50 mV up to −10 mV (Figs. 5*D* and 6*B*). At the experimental temperature of 21 °C, the process has a corner frequency of 500 Hz, equivalent to a time constant of 0.32 ms, but if the mechanism involves a voltage-dependent ion channel, the time constant could be fourfold faster at 27 °C. One possible ion channel is the voltage-dependent L-type (Cav1.3) Ca^{2+} channel, which, in hair cells, has the appropriate activation range and kinetics (4, 29) and is blocked by 2 mM $CoCl_2$. How Ca^{2+} entry might trigger motor elements, such as a nonmuscle myosin, and whether it would be sufficiently fast to explain the voltage-evoked motion are unknown. More work is needed to define the mechanism and distribution of the evoked movements.

1. A. C. Crawford, R. Fettiplace, An electrical tuning mechanism in turtle cochlear hair cells. *J. Physiol.* **312**, 377–412 (1981).
2. R. Fettiplace, Diverse mechanisms of sound frequency discrimination in the vertebrate cochlea. *Trends Neurosci.* **43**, 88–102 (2020).
3. M. S. Smotherman, P. M. Narins, The electrical properties of auditory hair cells in the frog amphibian papilla. *J. Neurosci.* **19**, 5275–5292 (1999).
4. A. J. Hudspeth, R. S. Lewis, Kinetic analysis of voltage- and ion-dependent conductances in saccular hair cells of the bull-frog, *Rana catesbeiana. J. Physiol.* **400**, 237–274 (1988).
5. Y. C. Wu, J. J. Art, M. B. Goodman, R. Fettiplace, A kinetic description of the calcium-activated potassium channel and its application to electrical tuning of hair cells. *Prog. Biophys. Mol. Biol.* **63**, 131–158 (1995).
6. J. Ashmore, Cochlear outer hair cell motility. *Physiol. Rev.* **88**, 173–210 (2008).
7. G. A. Manley, D. L. Kirk, C. Köppl, G. K. Yates, In vivo evidence for a cochlear amplifier in the hair-cell bundle of lizards. *Proc. Natl. Acad. Sci. U.S.A.* **98**, 2826–2831 (2001).
8. P. Martin, A. J. Hudspeth, Active hair-bundle movements can amplify a hair cell's response to oscillatory mechanical stimuli. *Proc. Natl. Acad. Sci. U.S.A.* **96**, 14306–14311 (1999).
9. P. Martin, D. Bozovic, Y. Choe, A. J. Hudspeth, Spontaneous oscillation by hair bundles of the bullfrog's sacculus. *J. Neurosci.* **23**, 4533–4548 (2003).
10. E. A. Rohtla, A. P. Russell, A. M. Bauer, Sounding off: Relationships between call properties, body size, phylogeny and laryngotracheal form of geckos. *Herpetologica* **75**, 175–197 (2019).
11. M. L. Gallo, C. Köppl, Spontaneous otoacoustic emissions in two gecko species, *Gekko gecko* and *Eublepharis macularius. J. Acoust. Soc. Am.* **99**, 1588–1603 (1996).
12. M. Gelfand, O. Piro, M. O. Magnasco, A. J. Hudspeth, Interactions between hair cells shape spontaneous otoacoustic emissions in a model of the Tokay gecko's cochlea. *PLoS One* **5**, e11116 (2010).
13. E. G. Wever, *The Reptile Ear* (Princeton University Press, 1978).
14. T. Holton, T. F. Weiss, Frequency selectivity of hair cells and nerve fibres in the alligator lizard cochlea. *J. Physiol.* **345**, 241–260 (1983).
15. C. Köppl, S. Authier, Quantitative anatomical basis for a model of micromechanical frequency tuning in the Tokay gecko, *Gekko gecko. Hear. Res.* **82**, 14–25 (1995).
16. M. E. Chiappe, A. S. Kozlov, A. J. Hudspeth, The structural and functional differentiation of hair cells in a lizard's basilar papilla suggests an operational principle of amniote cochleas. *J. Neurosci.* **27**, 11978–11985 (2007).
17. R. A. Eatock, G. A. Manley, L. Pawson, Auditory nerve activity in the Tokay gecko: I. Implications for cochlear processing. *J. Comp. Physiol.* **142**, 203–218 (1981).
18. F. Sams-Dodd, R. R. Capranica, Representation of acoustic signals in the eighth nerve of the Tokay gecko: I. Pure tones. *Hear. Res.* **76**, 16–30 (1994).
19. G. A. Manley, C. Köppl, M. Sneary, Reversed tonotopic map of the basilar papilla in *Gekko gecko. Hear. Res.* **131**, 107–116 (1999).
20. A. H. Griffing *et al.*, And thereby hangs a tail: Morphology, developmental patterns and biomechanics of the adhesive tails of crested geckos (*Correlophus ciliatus*). Proc. Biol. *Sci.* **288**, 20210650 (2021).
21. J. Snyder, L. Snyder, A. M. Bauer, Ecological observations on the gargoyle gecko, *Rhacodactylus auriculatus* (BAVAY, 1869), in southern New Caledonia. *Salamandra (Frankf.)* **46**, 37–47 (2010).
22. F. Dodd, R. R. Capranica, A comparison of anesthetic agents and their effects on the response properties of the peripheral auditory system. *Hear. Res.* **62**, 173–180 (1992).
23. X. Tan, M. Beurg, C. Hackney, S. Mahendrasingam, R. Fettiplace, Electrical tuning and transduction in short hair cells of the chicken auditory papilla. *J. Neurophysiol.* **109**, 2007–2020 (2013).
24. G. A. Manley, U. Sienknecht, C. Köppl, Calcium modulates the frequency and amplitude of spontaneous otoacoustic emissions in the bobtail skink. *J. Neurophysiol.* **92**, 2685–2693 (2004).
25. A. C. Crawford, R. Fettiplace, The mechanical properties of ciliary bundles of turtle cochlear hair cells. *J. Physiol.* **364**, 359–379 (1985).
26. A. J. Ricci, A. C. Crawford, R. Fettiplace, Active hair bundle motion linked to fast transducer adaptation in auditory hair cells. *J. Neurosci.* **20**, 7131–7142 (2000).
27. M. Beurg, X. Tan, R. Fettiplace, A prestin motor in chicken auditory hair cells: Active force generation in a nonmammalian species. *Neuron* **79**, 69–81 (2013).
28. P. A. Fuchs, T. Nagai, M. G. Evans, Electrical tuning in hair cells isolated from the chick cochlea. *J. Neurosci.* **8**, 2460–2467 (1988).
29. J. J. Art, R. Fettiplace, Variation of membrane properties in hair cells isolated from the turtle cochlea. *J. Physiol.* **385**, 207–242 (1987).
30. R. A. Eatock, G. A. Manley, Auditory nerve fibre activity in the Tokay gecko II. Temperature effect on tuning. *J. Comp. Physiol.* **142**, 219–226 (1981).
31. P. A. Fuchs, M. G. Evans, Potassium currents in hair cells isolated from the cochlea of the chick. *J. Physiol.* **429**, 529–551 (1990).
32. P. D. Langton, M. T. Nelson, Y. Huang, N. B. Standen, Block of calcium-activated potassium channels in mammalian arterial myocytes by tetraethylammonium ions. *Am. J. Physiol.* **260**, H927–H934 (1991).
33. L. Castelli, F. Tanzi, V. Taglietti, J. Magistretti, Cu^{2+}, Co^{2+}, and Mn^{2+} modify the gating kinetics of high-voltage-activated Ca^{2+} channels in rat palaeocortical neurons. *J. Membr. Biol.* **195**, 121–136 (2003).
34. H. E. Farris, C. L. LeBlanc, J. Goswami, A. J. Ricci, Probing the pore of the auditory hair cell mechanotransducer channel in turtle. *J. Physiol.* **558**, 769–792 (2004).
35. A. J. Ricci, Y. C. Wu, R. Fettiplace, The endogenous calcium buffer and the time course of transducer adaptation in auditory hair cells. *J. Neurosci.* **18**, 8261–8277 (1998).
36. H. J. Kennedy, M. G. Evans, A. C. Crawford, R. Fettiplace, Fast adaptation of mechanoelectrical transducer channels in mammalian cochlear hair cells. *Nat. Neurosci.* **6**, 832–836 (2003).
37. K. X. Kim, R. Fettiplace, Developmental changes in the cochlear hair cell mechanotransducer channel and their regulation by transmembrane channel-like proteins. *J. Gen. Physiol.* **141**, 141–148 (2013).
38. R. Fettiplace, K. X. Kim, The physiology of mechanoelectrical transduction channels in hearing. *Physiol. Rev.* **94**, 951–986 (2014).
39. S. Authier, G. A. Manley, A model of frequency tuning in the basilar papilla of the Tokay gecko, *Gekko gecko. Hear. Res.* **82**, 1–13 (1995).
40. K. P. Steel, The tectorial membrane of mammals. *Hear. Res.* **9**, 327–359 (1983).
41. D. Bozovic, A. J. Hudspeth, Hair-bundle movements elicited by transepithelial electrical stimulation of hair cells in the sacculus of the bullfrog. *Proc. Natl. Acad. Sci. U.S.A.* **100**, 958–963 (2003).
42. H. Ohmori, Mechano-electrical transduction currents in isolated vestibular hair cells of the chick. *J. Physiol.* **359**, 189–217 (1985).
43. A. B. Kroese, A. Das, A. J. Hudspeth, Blockage of the transduction channels of hair cells in the bullfrog's sacculus by aminoglycoside antibiotics. *Hear. Res.* **37**, 203–217 (1989).
44. M. J. Tunstall, J. E. Gale, J. F. Ashmore, Action of salicylate on membrane capacitance of outer hair cells from the guinea-pig cochlea. *J. Physiol.* **485**, 739–752 (1995).
45. A. Rüsch, U. Thurm, Spontaneous and electrically induced movements of ampullary kinocilia and stereovilli. *Hear. Res.* **48**, 247–263 (1990).
46. C. Griguer, J. Lehouelleur, J. Valat, A. Sahuquet, A. Sans, Voltage dependent reversible movements of the apex in isolated guinea pig vestibular hair cells. *Hear. Res.* **67**, 110–116 (1993).
47. F. Vranceanu *et al.*, Striated organelle, a cytoskeletal structure positioned to modulate hair-cell transduction. *Proc. Natl. Acad. Sci. U.S.A.* **109**, 4473–4478 (2012).
48. S. Ebrahim *et al.*, NMII forms a contractile transcellular sarcomeric network to regulate apical cell junctions and tissue geometry. *Curr. Biol.* **23**, 731–736 (2013).
49. J. Zheng *et al.*, Prestin is the motor protein of cochlear outer hair cells. *Nature* **405**, 149–155 (2000).
50. P. Dallos *et al.*, Prestin-based outer hair cell motility is necessary for mammalian cochlear amplification. *Neuron* **58**, 333–339 (2008).